AJR 2003; 181:861-866

Pictorial Essay

Contrast-Enhanced MR Angiography of Thoracic Vascular Malformations in a Pediatric Population

Filipe Caseiro-Alves[1,2], Paulo Gil-Agostinho[1], Graça Ramalheiro[3] and Pedro Gil-Agostinho[1]

[1] Imacentro, Clinica de Imagiologia Médica, Rua S.Teotónio, Lote 8, 5° Esq., 3000-377 Coimbra, Portugal.
[2] Faculdade de Medicina de Coimbra, Cadeira de Imagiologia, 3000-075 Coimbra, Portugal.
[3] Paediatric Cardiology Department, Hospital Pediátrico de Coimbra, Av. Bissaia Barreto, 3000 Coimbra, Portugal.

Received December 5, 2002; accepted after revision January 28, 2003.

Address correspondence to F. Caseiro-Alves (fcalves@netcabo.pt).

Introduction

Diagnostic gadolinium-enhanced MR angiography has been successfully used in the past few years for a vast array of medical indications [1]. With the new high-performance gradients that allow the use of an ultrashort TR and TE, three-dimensional (3D) data sets can now be acquired in a single breath-hold. Also, the new schemes for k-space reconstruction, such as the centric or elliptic-centric modes, ensure the most useful phase of reduced blood T1-weighted relaxation is easily captured, increasing the temporal

resolution necessary to image both arterial and venous structures [1, 2].

Performing contrast-enhanced MR angiography in pediatric patients, particularly neonates, poses additional problems because examinations are typically conducted with the patient under general anesthesia in a non-breath-hold fashion. Previous reports have shown the feasibility of using contrast-enhanced MR angiography in a pediatric population to study several vascular thoracic and abdominal abnormalities, mainly of the arterial system [2-5]. In addition, the ability to study malformations of the thoracic vasculature in neonates under general anesthesia and during spontaneous breathing has been described (Caseiro-Alves F et al., presented at the Radiological Society of North America meeting, December 2000). Our imaging group is working closely with a national referral center for pediatric cardiology and has already performed more than 100 of these procedures. All patients were examined with light anesthesia produced by inhalation of sevoflurane (Ultane, Abbott Laboratories, Amadora, Portugal). To date, no cases of severe adverse effects have been registered, even when imaging 1-day-old neonates with complex cyanotic congenital cardiopathy and blood oxygen saturation levels as low as 40-50%.

Technique

Images were generated in two magnetic fields (1 and 1.5 T) (Signa Horizon and Signa MRI EchoSpeed Plus, General Electric Medical Systems, Milwaukee, WI). A 3D fast gradient-echo sequence was performed in the coronal plane using a nominal slice thickness of 3.2 mm and a partition number selected depending on the anatomic area to cover. The choice of imaging coil depended on the size of the patient; the head transmitting-receiver coil was regularly used in infants who weighed less than 9 kg. The 3D sequence was acquired in 18-20 sec. It was launched after a fixed delay of 15 sec after the manual injection of a double dose (0.2 mmol/kg of body weight) of IV ionic gadopentetate dimeglumine (Magnevist, Schering, Berlin), and the contrast-generating k-space central lines were acquired during the first few seconds. The complete procedure including administration of anesthesia was concluded in approximately 10-15 min. Interpolated reconstruction was regularly applied to obtain a final number of slices multiplied by a factor of 2 or 4 without any penalty in acquisition time.

The native coronal two-dimensional slices (typically 80-120 images) were transferred to a diagnostic workstation (Advantage Windows 4.0, General Electric Medical Systems) for 3D postprocessing using maximum-intensity-projection and volume-rendering techniques.

Clinical Results

Corroborating the findings of previous reports that focused mainly on the arterial thoracic vessels [6-8], this pictorial essay shows the potential uses of contrast-enhanced MR angiography for the diagnosis of vascular thoracic malformations in both the arterial and venous systems in pediatric patients. These uses make the technique a valuable diagnostic tool with the potential to replace the more invasive digital subtraction angiography.

Aortic Arch Anomalies

Aortic Coarctation

Aortic coarctation (Figs. 1A, 1B, and 1C) is a narrowing of the aortic arch generally at the level of the ductus arteriosus. This anomaly can be diffuse, causing tubular hypoplasia of the aortic arch (the infantile type), or segmental (the adult type).

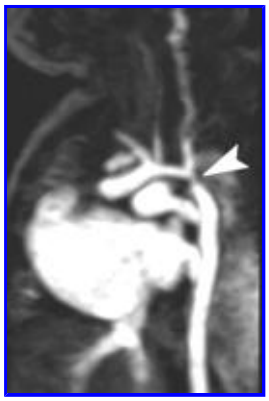

View larger version (96K):
[in this window]
[in a new window]
[as a PowerPoint slide]

Fig. 1A. ð Spectrum of findings in selected cases of aortic coarctation (*arrowhead*, **A** and **B**) shown on contrast-enhanced MR angiograms obtained using three-dimensional techniques. Parasagittal oblique maximum-intensity-projection image of 2-day-old female neonate shows simple isolated coarctation at its typical location.

View larger version (78K):
[in this window]
[in a new window]
[as a PowerPoint slide]

Fig. 1B. ð Spectrum of findings in selected cases of aortic coarctation (*arrowhead*, **A** and **B**) shown on contrast-enhanced MR angiograms obtained using three-dimensional techniques. Maximum-intensity-projection image of 1-year-old male infant displays collaterals (intercostals) developed for arterial circulation.

Fig. 1C. ð Spectrum of findings in selected cases of aortic coarctation (*arrowhead*, **A** and **B**) shown on contrast-enhanced MR angiograms obtained using three-dimensional techniques. Posterior oblique volume-rendered image of 28-day-old male neonate shows

View larger version (131K):
[in this window]
[in a new window]
[as a PowerPoint slide]

severe coarctation associated with hypoplastic distal aortic arch.

Aortic Arch Interruption

Aortic arch interruption (Fig. 2) is a complete separation of the ascending and descending segments of the thoracic aorta. According to Weinberg [8], aortic arch interruption can be classified as type A, when the interruption is distal to the left subclavian artery origin; type B, when between the carotid and left subclavian arteries; or type C, when located in the proximal aortic arch between the carotid arteries.

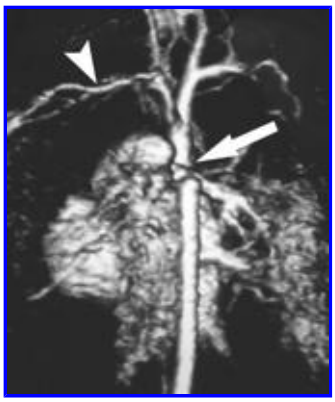

View larger version (127K):
[in this window]
[in a new window]
[as a PowerPoint slide]

Fig. 2. ð 2-day-old male neonate with aortic arch interruption. Contrast-enhanced three-dimensional MR angiogram obtained using volume-rendering technique reveals type A interruption of aortic arch (*arrow*). Arrowhead = left subclavian artery.

Double Aortic Arch

Double aortic arch (Figs. 3A, and 3B) corresponds to the persistence of both fetal aortic arches and has several variants: both arches may be widely patent or one of the two arches may became hypoplastic or even atretic (usually the one on the left side). The trachea and esophagus may be completely surrounded by the aortic arches, which results in a vascular ring. Because some degree of tracheomalacia is usually associated with this condition, clinical signs associated with vascular compression such as stridor or vomiting may be present.

View larger version (109K):
[in this window]
[in a new window]
[as a PowerPoint slide]

Fig. 3A. ð Contrast-enhanced three-dimensional MR angiograms reveal double aortic arch (*arrows*) that gave rise to stridor in 75-day-old male infant. Coronal oblique maximum-intensity-projection image shows early bifurcation of ascending aorta.

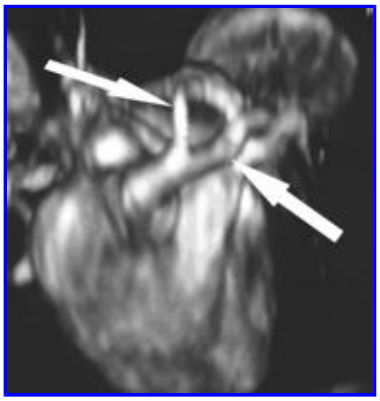

View larger version (142K):
[in this window]
[in a new window]
[as a PowerPoint slide]

Fig. 3B. ð Contrast-enhanced three-dimensional MR angiograms reveal double aortic arch (*arrows*) that gave rise to stridor in 75-day-old male infant. Superior volume-rendered image shows double aortic arch.

Aberrant Right Subclavian Artery

An aberrant right subclavian artery (Fig. 4) can give rise to the clinical sign of dysphagia lusoria. In patients with this malformation, the right subclavian artery (arteria lusoria) crosses the superior mediastinum behind the esophagus and potentially causes compression over its posterior wall.

Fig. 4. ð Posterior contrast-enhanced three-dimensional MR angiogram obtained using volume-rendering technique shows aberrant right subclavian artery (*arrow*) in 10-day-old male neonate.

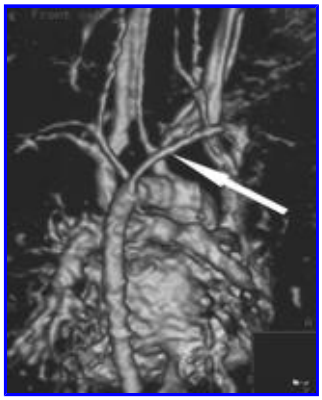

View larger version (133K):
[in this window]
[in a new window]
[as a PowerPoint slide]

Right Aortic Arch with Retroesophageal Kommerell Diverticulum

In patients with this malformation, the aortic arch has a right-sided configuration and the first emerging branch is the left carotid artery. A retroesophageal vessel of variable size (the so-called Kommerell diverticulum) gives rise to the left subclavian artery (Fig. 5). This abnormal pouch of variable length corresponds to the atretic portion of the left fetal arch and is connected to the left ductus arteriosus or ligamentum arteriosum. This vessel arrangement may also behave as a vascular ring that produces dysphagia.

View larger version (155K):
[in this window]
[in a new window]
[as a PowerPoint slide]

Fig. 5. ð Posterior contrast-enhanced three-dimensional MR angiogram obtained using volume-rendering technique shows incomplete double aortic arch forming retroesophageal Kommerell diverticulum (*arrowhead*) in 35-day-old male infant. Left subclavian artery (*arrow*) can be seen arising in "diverticular" component of vascular ring.

Right Aortic Arch with Mirror Image of the Supraaortic Vessels

As the name implies, the vessels are arranged as a mirror image of the left aortic arch (Figs. 6A, and 6B). This condition is one of the most common aortic arch abnormalities and is frequently associated with other congenital cardiopathy.

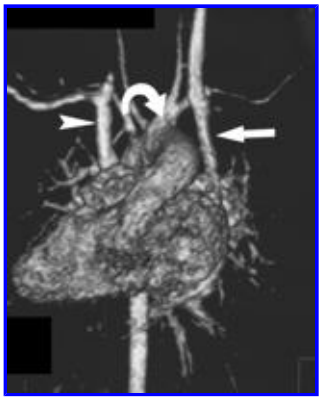

View larger version (103K): [in this window] [in a new window] [as a PowerPoint slide]

Fig. 6A. ð Contrast-enhanced three-dimensional MR angiograms obtained using volume-rendering technique show right aortic arch with mirror image of supraaortic vessels in 12-day-old female neonate with dextrocardia. Anterior (**A**) and posterior (**B**) images show right aortic arch with mirror image of supraaortic vessels and also reveal double superior vena cava: straight arrow points to left superior vena cava; arrowhead, to right superior vena cava; and curved arrow, to left brachiocephalic trunk.

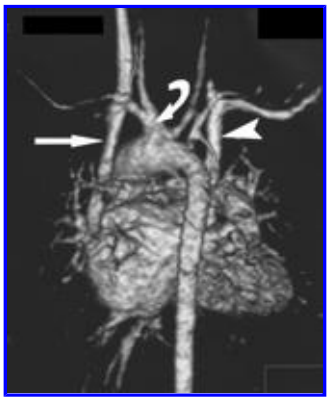

View larger version (109K): [in this window] [in a new window] [as a PowerPoint slide]

Fig. 6B. ð Contrast-enhanced three-dimensional MR angiograms obtained using volume-rendering technique show right aortic arch with mirror image of supraaortic vessels in 12-day-old female neonate with dextrocardia. Anterior (**A**) and posterior (**B**) images show right aortic arch with mirror image of supraaortic vessels and also reveal double superior vena cava: straight arrow points to left superior vena cava; arrowhead, to right superior vena cava; and curved arrow, to left brachiocephalic trunk.

Abnormalities of the Pulmonary Arteries

There is a broad spectrum of possible congenital malformations of the pulmonary trunk and major vessels, ranging from isolated stenosis to severe hypoplasia or even atresia. In addition to revealing the presence or absence of the major pulmonary trunk and branches, contrast-enhanced MR angiography allows the direct measurement of the diameter of these pulmonary vessels (Fig. 7). These measurements are important in determining whether a surgical shunt (e.g., Blalock-Taussig shunt) can be created to correct the malformation because creating this shunt may not be feasible if the pulmonary arteries measure less than 3 mm.

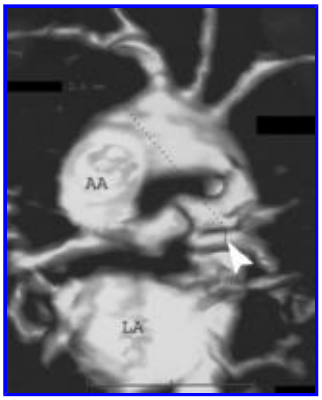

View larger version (115K):
[in this window]
[in a new window]
[as a PowerPoint slide]

Fig. 7. ð 1-day-old male neonate with hypoplasia of pulmonary artery branches. Contrast-enhanced three-dimensional MR angiogram obtained using volume-rendering technique allows diameter of vessel to be measured. Dotted line corresponds to diameter measurement of left pulmonary artery (2.6 mm). AA = ascending aorta, LA = left atrium, arrowhead = left pulmonary artery.

Abnormal Venous Connections

Pulmonary

Abnormal pulmonary venous connections can be divided into partial abnormal venous return, such as that seen in patients with scimitar syndrome (Fig. 8), and total abnormal venous return. The latter category can be further subdivided: the supracardiac type, in which a vertical vein draining the common pulmonary veins joins the left innominate vein to open into the superior vena cava (Figs. 9A and 9B); the infracardiac type, in which the pulmonary veins drain directly into the coronary sinus; the common type, in which the pulmonary veins drain into the right atrium; and the rare infradiaphragmatic type, in which the pulmonary veins join in a common trunk to drain into the portal vein (Fig. 9C).

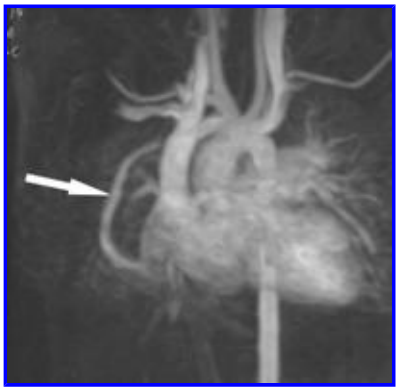

View larger version (132K):
[in this window]
[in a new window]
[as a PowerPoint slide]

Fig. 8. ð 3-year-old boy with partial abnormal pulmonary venous return. Anterior contrast-enhanced three-dimensional MR angiogram obtained using maximum-intensity-projection technique reveals connection of right pulmonary vein to inferior vena cava (*arrow*), indicating scimitar syndrome.

View larger version (127K):
[in this window]
[in a new window]
[as a PowerPoint slide]

Fig. 9A. ð Two types of total abnormal pulmonary venous return shown on contrast-enhanced three-dimensional MR angiography. Coronal image of 1-day-old male neonate reveals supracardiac type of total abnormal pulmonary venous return: common vertical vein (*arrow*) drains all pulmonary veins.

View larger version (151K):
[in this window]
[in a new window]
[as a PowerPoint slide]

Fig. 9B. ð Two types of total abnormal pulmonary venous return shown on contrast-enhanced three-dimensional MR angiography. Volume-rendered image of same patient as shown in **A** reveals connection of pulmonary veins (*arrowheads*) to common vertical vein (*arrow*) better than **A**.

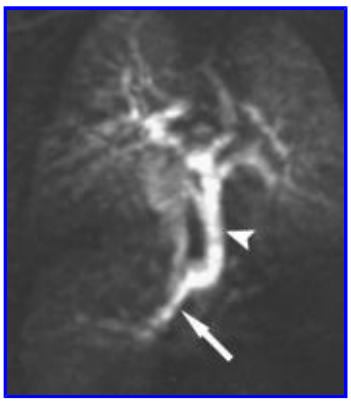

View larger version (111K):
[in this window]
[in a new window]
[as a PowerPoint slide]

Fig. 9C. ð Two types of total abnormal pulmonary venous return shown on contrast-enhanced three-dimensional MR angiography. Coronal image of 3-day-old male neonate with infracardiac type of total abnormal venous return shows pulmonary veins converge toward single abnormal channel (*arrowhead*) that crosses mediastinum to drain into left portal vein (*arrow*).

Systemic

These conditions are variants of the normal systemic venous drainage and do not produce clinical symptoms or signs. The most common variant is a persistent left superior vena cava connecting either to the right atrium in 92% of cases (Figs. 10A, and 10B) or to the left atrium in the remaining cases. The depiction of a persistent left superior vena cava may influence the choice of the side on which to perform a surgical pulmonary-systemic shunt.

View larger version (89K):
[in this window]
[in a new window]
[as a PowerPoint slide]

Fig. 10A. ð 2-year-old boy with abnormal systemic venous connection shown on contrast-enhanced three-dimensional MR angiography. Lateral maximum-intensity-projection image (**A**) and anterior volume-rendered image (**B**) show persistent left superior vena cava (*arrow*) connects to coronary sinus (*arrowhead*, **A**).

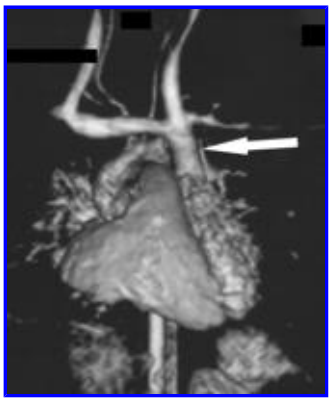

View larger version (117K):
[in this window]
[in a new window]
[as a PowerPoint slide]

Fig. 10B. ð 2-year-old boy with abnormal systemic venous connection shown on contrast-enhanced three-dimensional MR angiography. Lateral maximum-intensity-projection image (**A**) and anterior volume-rendered image (**B**) show persistent left superior vena cava (*arrow*) connects to coronary sinus (*arrowhead*, **A**).

Follow-Up for Corrected Vascular Abnormalities

Contrast-enhanced MR angiography can also be useful for the Top

evaluation of patients who have undergone surgery to correct a vascular abnormality. Although surgically created shunts are small, contrast-enhanced MR angiography can reveal whether the shunt is patent, as we have observed in patients with Blalock-Taussig shunts (Figs. 11A, and 11B). In addition, the postsurgical status of a surgically corrected aortic coarctation can be monitored by obtaining direct measurements of the vessel diameter (Fig. 12).

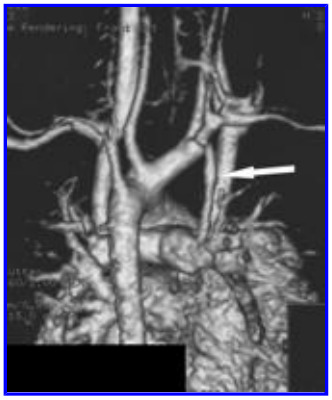

View larger version (127K):
[in this window]
[in a new window]
[as a PowerPoint slide]

Fig. 11A. ð Contrast-enhanced MR angiograms obtained at postsurgical follow-up of 3-year-old girl who underwent placement of modified Blalock-Taussig shunt. Posterior volume-rendered image (**A**) and coronal maximum-intensity-projection image (**B**) show patency of modified Blalock-Taussig shunt (*arrow*).

View larger version (126K):
[in this window]
[in a new window]
[as a PowerPoint slide]

Fig. 11B. ð Contrast-enhanced MR angiograms obtained at postsurgical follow-up of 3-year-old girl who underwent placement of modified Blalock-Taussig shunt. Posterior volume-rendered image (**A**) and coronal maximum-intensity-projection image (**B**) show patency of modified Blalock-Taussig shunt (*arrow*).

Fig. 12. ð 4-year-old boy in whom recoarctation of aorta was suspected on basis of findings on Doppler sonograms (not shown) that revealed 15-mm-Hg systolic pressure gradient between two segments of aorta. This posterior oblique contrast-enhanced MR angiogram obtained using volume-rendering technique was used to calculate aortic diameter.

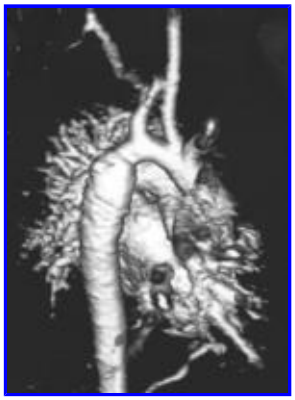

View larger version
(107K):
[in this window]
[in a new window]
[as a PowerPoint slide]

References

1. Joarder R, Gedroye WM. Magnetic resonance an giography: the state of the art. *Eur Radiol*2001; 11:446 -453[Medline]
2. Holmqvist C, Larsson E-M, Stahlberg F, Laurin S. Contrast-enhanced thoracic 3D-MR angiography in infants and children. *Acta Radiol* 2001;42:50 -58 [Medline]
3. Lam WW, Chan JH, Hui Y, Chan F. Non-breathhold gadolinium-enhanced MR angiography of the thoracoabdominal aorta: experience in 18 children. *AJR* 1998;170:478 -480[Free Full Text]
4. Teo EL, Strouse PJ, Prince MR. Applications of magnetic resonance imaging and magnetic reso nance angiography to evaluate the hepatic vasculature in the pediatric patient. *Pediatr Radiol*1999; 29:238 -243[Medline]
5. Neimatallah MA, Ho VB, Dong Q, et al. Gadolin ium-enhanced 3D magnetic resonance angiogra phy of the thoracic vessels. *J Magn Reson Imaging* 1999;10:758 -770[Medline]
6. Krinsky GA, Reuss PM, Lee VS, Carbognin G, Rofsky NM. Thoracic aorta: comparison of sin gle-dose breath-hold and double-dose non-breathhold gadolinium-enhanced three-dimensional MR angiography. *AJR* 1999;173:145 -150[Abstract/Free Full Text]
7. Krinsky G. Gadolinium-enhanced three-dimensional magnetic resonance angiography of the thoracic aorta and arch vessels. *Invest Radiol* 1998;33:587 -605[Medline]
8. Weinberg PM. Interrupted aortic arch. In: Moss AJ, Adams FH, Emmanouilides GC, eds. *Moss and Ad ams' heart disease in infants, children, and adoles cents: including the fetus and young adult,* 5th ed. Philadelphia: Williams & Wilkins, 1995:828 -832

This article has been cited by other articles:

S.-F. Ko, C.-D. Liang, C.-C. Huang, S.-H. Ng, M.-J. Hsieh, J.-P. Chang, and M.-C. Chen
Clinical feasibility of free-breathing, gadolinium-enhanced magnetic resonance angiography for assessing extracardiac thoracic vascular abnormalities in young children with congenital heart diseases.
J. Thorac. Cardiovasc. Surg., November 1, 2006; 132(5): 1092 - 1098.
[Abstract] [Full Text] [PDF]